Synthesis, Characterization, and Biological Activity Evaluation of Magnetite-Functionalized Eugenol

Franciele da Silva Bruckmann
Universidade Franciscana
Altevir Rossato Viana
Universidade Franciscana
Leonardo Quintana Soares Lopes
Universidade Federal de Santa Maria
Roberto Christ Vianna Santos
Universidade Federal de Santa Maria
Edson Irineu Muller
Universidade Federal de Santa Maria
Sergio Roberto Mortari
Universidade Franciscana
Cristiano Rodrigo Bohn Rhoden (cristianorbr@gmail.com)
Universidade Franciscana https://orcid.org/0000-0001-6171-4224

Research Article

Keywords: Magnetic, nanoparticles, Essential oil, Pharmacological activities

Posted Date: November 1st, 2021

DOI: https://doi.org/10.21203/rs.3.rs-1025029/v1

Abstract

In this work, we report, for the first time, the magnetite-functionalization and biological evaluation of eugenol by the co-precipitation method employed only Fe^{2+} under mild conditions and control from the amount of the incorporated magnetite. Magnetic nanoparticles were characterized by scanning electron microscopy (SEM), X-ray diffraction (XRD), Fourier transform infrared (FTIR), and hydrodynamic size distribution (Zetasizer). SEM images showed that EUG·Fe_3O_4 is 200 nm in size and similar in shape to a nanoflower. The FTIR spectrum confirmed the presence of characteristic EUG and Fe_3O_4 bands in the EUG·Fe_3O_4 sample, while the XRD analysis showed that the magnetite functionalization with eugenol slightly affected the Fe_3O_4 crystal structure. The *in vitro* safety profile and cytotoxicity of free eugenol, magnetite pristine, EUG·Fe_3O_4 1:1, EUG·Fe_3O_4 1:5, and EUG·Fe_3O_4 1:10 was investigated using human cell lines (keratinocytes and melanoma). The results demonstrate the high biocompatibility of EUG·Fe_3O_4 in HaCat cells and the greater specificity for the A375 cell line. Furthermore, the magnetite-functionalized with eugenol decreased the toxic effects of free eugenol on healthy cells. Antibacterial tests were performed in different bacterial strains. The experimental data showed that among the magnetic compounds, the microorganisms were only sensitive to treatment with EUG·Fe_3O_4 1:1. Regarding the antibiofilm activity assay, it can be observed that only the EUG·Fe_3O_4 caused a significant decrease in biomass when compared to the positive control. Finally, it can be concluded that EUG·Fe_3O_4 proves to be a potential candidate for future studies for drug delivery of cancer and bacterial infections treatments.

1 Introduction

Recently, the development of drug delivery systems has been widely investigated due to the limitations of conventional treatments, such as insolubility, low stability, toxicity, and serious adverse effects [1, 2]. In addition, some drugs have difficulty in reaching distant organs. Thus, nanotechnology through atomic and molecular manipulation of materials enables the synthesis of nanoparticles with new properties and applications, allowing its application in diverse areas [3, 4, 5]. A variety of nanoparticles have been developed as a vehicle for drug targeting that can show different sizes, shapes, and chemical compositions [6]. Among nanoparticulated systems, magnetic nanoparticles (MNPs) have been demonstrated excellent nanoplatforms for drug delivery due to unique properties such as biocompatibility, easy preparation, and functionalization [7, 8].

Particularly, superparamagnetic iron oxide nanoparticles (SPIONs) (Fe_3O_4 and γ-Fe_2O_3) have been promising in biological activity studies due to their easy metabolism, biodegradability, and biocompatibility. Superparamagnetic nanoparticles have advantages over other metallic nanoparticles. The fact that SPIONs exhibit magnetic behavior only approaching a magnet decrease clot formation and biological agglomeration [9, 10].

Likewise, MNPs are able to enhance the pharmacological effect of drugs, bioactive compounds, and essential oils. Newly, Shahabadi et al. [7] developed magnetic core-shell nanoparticle-containing eugenol

(EUG) with antitumoral and antibacterial activities superior to free EUG.

Essential oils are products from the secondary metabolites of plants and are known to have several therapeutic properties. The EUG (4-allyl-2-methoxyphenol) is a phenolic compound, with hydrophilic characteristics and the majority compound of clove oil (*Syzygium aromaticum*), characterized for present excellent antibacterial, antiproliferative, antioxidant, and anti-inflammatory activities [7, 11, 12].

In this work, we report a simple method of functionalization of eugenol with control of amount incorporated magnetite as well as characterization of the synthesized nanocomposites. Posteriorly, the biological properties of the EUG·Fe_3O_4 were investigated through *in vitro* a safety profile, antibacterial, antibiofilm, and antitumor activity.

2 Materials And Methods

2.1 Synthesis of magnetite-functionalized eugenol with different proportions magnetite (EUG·Fe_3O_4)

The magnetite-functionalized eugenol was carried out as described by Rhoden et al. [3]. In a 250 mL round-bottom flask containing 100 mL of ultrapure water previously deoxygenated, 100 mg of EUG (Sigma-Aldrich®) were added with different amounts of Ferrous Sulphate heptahydrate ($FeSO_4 \cdot 7H_2O$) (Sigma-Aldrich®) i.e., 100 mg for EUG·Fe_3O_4 1:1, 500 mg for EUG·Fe_3O_4 1:5, and 1000 mg for EUG·Fe_3O_4 1:10. Sequentially ammonium hydroxide (Synth®) was added until the mixture reaches an oxidizing pH (pH ≈ 10.0). Afterwards the mixture was submitted to ultrasonic irradiation (Elma, power 150W) for 60 minutes. Sequentially, the solution was poured with the assistance of magnetic field and the solid was consecutively washed with water. Subsequently the material was dried at room temperature (RT).

2.2 Cell culture

In this study, A375 (human melanoma) and HaCat (human keratinocyte) cell lines procured from Rio de Janeiro Cell Bank were employed. The cells were cultivated in Dulbecco's modified eagles' medium (DMEM) with 10% fetal bovine serum and 1% penicillin/streptomycin. For toxicity assay, the cells were seeded in 96-well plates, at a concentration of $2x10^4$ to plate, under a controlled atmosphere (37 ºC, 5% CO_2, and 95% relative humidity). The cells were incubated with different treatments (free EUG, pristine Fe_3O_4, EUG·Fe_3O_4 1:1, EUG·Fe_3O_4 1:5, EUG·Fe_3O_4 1:10), with concentrations varying between 1-100 $\mu g.mL^{-1}$ for 24 hours.

2.3 MTT assay

The cytotoxic effects of magnetic nanoparticles were investigated through of 3-(4,5-dimethylthiazol-2-yl)-2,5-diphenyl tetrazolium bromide (MTT) assay using technique propose by Mosmann [13]. After 24 hours, a solution of 5 $mg.mL^{-1}$ of the reagent was prepared diluted in 1x phosphate-buffered saline (PBS)

(Prolab®) and subsequently added 20 µL per well in the 96-well plates maintained at 37 ºC under CO_2 atmosphere for four hours. The supernatant was then removed and add 200 µL of dimethyl sulfoxide (DMSO) (Synth®) to solubilize the crystals formed. Finally, the absorbance was measure at a wavelength of 570 nm using a microplate reader (SpectraMax® i3x – Molecular Devices).

2.4 Neutral Red assay

The neutral red test was based on the initial protocol described by Borenfreund and Puerner [14], following the methodology described by Bruckmann et al. [8]. After 24 hours, the supernatant was removed and, a culture medium without serum was added to fetal bovine with the neutral red reagent at a concentration of 40 µg.mL^{-1}. The cells remained for 4 hours of incubation in the CO_2 oven in contact with the reagent. Afterward, the supernatant was removed, cells were washed with 1x PBS to remove excess unreacted reagent incorporated by them. Finally, a lysis solution containing 50% ethanol (Synth®), 49% distilled water, and 1% acetic acid (Synth®) for cell lysis and dye release to read absorbance at a wavelength of 540 nm.

2.5 LDH assay

The activity of the lactate dehydrogenase (LDH) enzyme released into the extracellular medium was measured in the supernatant of the culture wells using the non-radioactive colorimetric assay CyToTox96 according to the manufacturer's instructions. For the LDH assay, a volume of 100 µL supernatant + 100 µL substrate was transferred to another 96-well plate. After 30 minutes of incubation at room temperature, absorbance was measured at 490 nm in a microplate reader (SpectraMax® i3x – Molecular Devices).

2.5 Microorganisms

The following microorganisms were used in the experiments: *Staphylococcus aureus* (ATCC 29213), *Escherichia coli* (ATCC 35218), *Enterococcus faecalis* (ATCC 29212) and *Pseudomonas aeruginosa* (PAO1). The strains were purchased from the American Type Culture Collection (ATCC). The samples were inoculated on Brain Heart Infusion broth (BHI) and incubated for 24 h. After that, they were seeded on Nutrient agar and incubated for 24 h at 37 ºC. From the grown colonies, the suspensions in NaCl at 0.9% corresponding to the 0.5 at McFarland scale (1.5x10^8 CFU/mL^{-1}) were produced.

2.6 Disc diffusion

The antimicrobial activity was initially evaluated by the disc diffusion technique, as described previously by Bauer et al [15]. The microorganisms were seeded in petri dishes with Mueller Hinton agar and three discs with each compound (EUG, Fe_3O_4, EUG·Fe_3O_4 1:1, EUG·Fe_3O_4 1:5, EUG·Fe_3O_4 1:10 were added on the agar surface. The plates were incubated for 24 h at 37 ºC and, afterwards, the inhibition zones were measured in millimeters (mm). The surfactant (Tween 80) used to dissolve some compounds was also tested. The experiment was performed in triplicates and in two independent experiments.

2.7 Minimal inhibitory and bactericidal concentration

The minimal inhibitory concentration (MIC) was determined by microdilution method in 96 well-plates according to Clinical and Laboratory Standards Institute (CLSI) [16] with modifications. Different concentrations of testes compounds (EUG, Fe_3O_4, EUG·Fe_3O_4 1:1, EUG·Fe_3O_4 1:5, EUG·Fe_3O_4 1:10) were added in wells with Mueller Hinton broth (MHB) and the suspension with microorganisms. Positive control was considered the well with only the suspension and MHB, while the negative control was only MHB. Afterwards, the plates were incubated for 24 h at 37 ºC. The assay was performed in triplicate. The assay was revealed with 2,3,5-triphenyl tetrazolium chloride, which develops a red color in the microbial grown. The lowest concentration that doesn't show change in color was considered as MIC. To determine the minimal bactericidal concentration (MBC), an aliquot of 1 µL was taken of each well, seeded on Nutrient agar plate and incubated for 24 h. After the incubation, the colonies were identified and the lowest concentration that did not demonstrated microbial growth was considered the MBC.

2.8 Biofilm formation and treatment

The antibiofilm potential was evaluated against the strain *P. aeruginosa* PAO1. The method used to this assay was described previously Manner et al. [17] with modifications. To biofilm formation, fresh exponentially grown culture of *P. aeruginosa* was diluted to be 10^8 CFU/mL, and 20 µL was added to 96-well plates (Nunclon™ D surface, Nunc, Roskilde, Denmark), containing 100 µL of BHI broth. The plate was incubated in 37 ºC for 24 h. After formation of the biofilm, the treatment was performed and incubated for 24 h in a condition of 37 ºC. The treatment was performed with MBC of tested compounds. A positive control was performed containing only BHI broth and the *P. aeruginosa* strain while the negative control was just BHI broth.

2.9 Quantification of biofilm biomass

The biomass of treated biofilm was quantified by method previous described by Lopes et al. [18]. The supernatant was removed and gently washed three times with distilled water, fixing with 95% of methanol and staining with 150 µL of 0.1% of crystal violet for 10 min at RT. After incubation, the well-plates were washed with distilled water, and ethanol 95% was added to dissolve the coloring after 15 min. After that, 100 µL were transferred into another plate to measure spectrophotometrically at 570 nm to crystal violet in spectrophotometer (TP-Reader; ThermoPlate, Goiás, Brazil).

2.10 Statistical analysis

Cytotoxicity analysis in HaCat and A375 cell lines of magnetic nanoparticles was performed using GraphPad Prism. The treatments were compared by one-way analysis of variance (ANOVA) was performed followed by Tukey's post hoc test. Statistically different values were considered with $p < 0.05$ (*), $p < 0.01$ (**), and $p < 0.001$ (***). The results of quantification of biofilm biomass were analyzed using the ANOVA followed by the Dunnet test was used considering values $p < 0.05$ (*) statistically significant compared with the Positive Control. Data were expressed as the Mean ± Standard deviation.

3 Results And Discussion

3.1 Characterization of magnetic nanoparticles

3.1.1 Fourier Transform Infrared Spectroscopy (FTIR)

The equipment used to characterize the magnetic nanoparticles and eugenol was Perkin-Elmer FTIR, model Spectro One. KBr disc method was used to record the spectra in spectral region between 4000 and 400 cm^{-1}. The infrared spectra (FTIR) of the free eugenol, magnetite pristine, and EUG·Fe_3O_4 are shown in Fig. 1.

In the FTIR spectrum of Fe_3O_4, it is possible to verify a band of vibration at 602 cm^{-1} typical of bonding Fe-O. The bands at 3443 cm^{-1} and 1633 cm^{-1} are attributed to the O-H stretching and vibration resulting from the absorption of water molecules [8].

For the spectrum of free eugenol, a characteristic band is observed around 3462 cm^{-1}, referring to the O-H bond in 2838 cm^{-1} the absorption peak corresponds to the stretching of the C-H bond. In the 1600-1500 cm^{-1} region, the peaks refer to the C=C bond, and the sharp peaks in the 1200-700 cm^{-1} region are due to the C=C bonds of the aromatic ring [7, 19].

In the spectrum of EUG·Fe_3O_4, in addition to the peaks remaining constant, a more intense peak is observed around 600 cm^{-1}, referring to Fe-O binding confirming the functionalization of eugenol with Fe_3O_4 [3].

3.1.2 X-ray diffraction (XRD)

Bruker Optics D2 Advance USA equipment was used for the characterization using X-ray diffraction (XRD) to determine the crystalline phases of the samples. Fig. 2 shows the XRD referring to the magnetite, and magnetite-functionalized eugenol, which demonstrates the characteristic peak of these nanoparticles.

The figure above show XRD patterns of magnetic nanoparticles synthetized in this work. In the diffractogram of the Fe_3O_4 pristine, it is possible to verify the crystal planes at $2\theta \approx 30º$, 35º 45º, 57º, and 62º, which corresponds to the characteristic diffraction interference of magnetite [7]. For the XRD of EUG Fe_3O_4, it can be observed that the functionalization of eugenol with magnetite caused a decrease in the intensity of the diffraction peaks. The partial suppression of the peaks indicates that eugenol presence slightly affected the crystal structure of the magnetite [3, 8].

3.1.3 Scanning electron spectroscopy (SEM) and Energy dispersive X-ray spectroscopy (EDS)

The morphology of magnetite functionalized eugenol and the elemental analysis of the nanoparticle was obtained by Scanning electron microscope (SEM) (Sigma 300 VP Carl Zeiss), and Energy dispersive X-ray spectroscopy (EDS) (Quantax 200-Z10, Bruker). Fig. 3 (a-b) shows the SEM image and EDS (c) of the eugenol and magnetic nanoparticles (EUG·Fe_3O_4).

The morphological structure and size of the magnetic eugenol nanoparticles were measured according to the SEM image. Fig. 3 (a) and (b) show SEM images of EUG·Fe_3O_4 at different scales.

As can be observed in the SEM images, the Fe_3O_4 deposited on the eugenol surface has a spherical shape, and the nanocomposite produced exhibited a morphology nanoflower-like and size particle of 200 nm [3, 20, 21].

Through the EDS analysis (Fig. 3c), it was possible to verify the presence of Fe (11.15%), C (46.97%), and O (41.31%) as the main chemical elements in the sample. Furthermore, the low relatively S percentage (0.57%) can be attributed to the residue of the iron salt ($FeSO_4$) used in the reaction.

3.1.4 Hydrodynamic size of the magnetite-functionalized eugenol

The size distribution of EUG·Fe_3O_4 1:1, EUG·Fe_3O_4 1:5, and EUG·Fe_3O_4 1:10 were analyzed using the Zetasizer®, nano-ZS model ZEN 3600, Malvern.

The average particle size distributions for EUG·Fe_3O_4 1:1, EUG·Fe_3O_4 1:5 and, EUG·Fe_3O_4 1:10 were 2.32, 185.3, and 190.1 nm, respectively, as shown in Fig. 4 (a-c). From hydrodynamic size profiles, it is possible to assume that the average size of nanoparticles rises directly with the amount of the Fe^{2+} employed in synthesis. The increase of the size distribution of magnetite-functionalized eugenol could be related to the tendency of formation aggregates due to the critical diameter of nanoparticles [22].

3.2 Cytotoxicity evaluation

3.2.1 3-(4,5-dimethylthiazol-2-yl)-2,5-diphenyl tetrazolium bromide (MTT) assay

The MTT test 3-(4,5-dimethylthiazol-2yl)-2,5-diphenyl tetrazolium bromide is a colorimetric test used to assess cell viability. Fig. 5 (a-b) represents the results of the MTT assay after 24 h treatment of HaCat and A375 cell lines, at a concentration of $2x10^4$ well, cultured in a 96-well plate and treated with free EUG, and EUG·Fe_3O_4 with different concentrations and proportions of incorporated magnetite, in triplicates.

For the MTT assay, it is possible to observe a significant viability decrease in the HaCat cell line with 10 $\mu g.mL^{-1}$ of the free EUG, while for A375 cells was necessary only 3 $\mu g.mL^{-1}$. Meanwhile, for all treatments of magnetite-incorporated eugenol, those confirming that the functionalization of eugenol offers protection against cytotoxic in healthy cells damage caused for free oil.

However, tumor cells were more sensitive to treatments of the magnetite-functionalized eugenol (EUG·Fe_3O_4 1:1, EUG·Fe_3O_4 1:5 and, EUG·Fe_3O_4 1:10).

Figure 6 (a-b) shows the viability of HaCat and A375 cells treated with magnetite pristine after 24 h of contact, respectively.

After 24 h of treatment at concentrations of 1, 3, 10, 30, and 100 μg.mL^{-1}, Fe_3O_4 pristine showed different toxicity against HaCat and A375 cell lines compared to free EUG. For the keratinocytes cell line, a significant decrease in viability is observed only at the highest concentrations tested (30-100 μg.mL^{-1}), which correspond to about 80% viable cells.

In contrast, for melanoma lineage from the lowest concentration, the cell viability rate decreases, in a dose-dependent manner, presenting statistical significance, as shown by Fig. 6b, in all dilutions of the magnetite [8].

3.2.2 Colorimetric viability assay from the neutral red vital dye

Figure 7 (a-b) shown the results of the cellular toxicity of the free eugenol and magnetite-functionalized eugenol employing the neutral red colorimetric assay under the same treatment conditions of the HaCat and A375 cell lines described in the cell culture item of the materials and methods assignment.

Through the neutral red (NR) colorimetric assay, a significant decrease in the viability of HaCat cells was observed at the highest concentrations (30 and 100 μg.mL^{-1}) in all treatments, except for EUG·Fe_3O_4 1:1, which showed cytotoxic effects only in the concentration of 100 μg.mL^{-1}.

However, in human melanoma cells, the action of nanoparticles was more evident, demonstrating that the materials offer better specificity against the tumor lineage, for instance, the highest concentration of free eugenol, EUG·Fe_3O_4 1:1, EUG·Fe_3O_4 1:5, and EUG·Fe_3O_4 1:10 reduced the number of viable cells to 46, 64, 54, and 44%, respectively.

Figure 8 (a-b) shows the viability of HaCat and A375 cells treated with magnetite pristine after 24 h of contact using the NR assay, respectively.

Confirming the MTT results (Fig. 5), only the highest concentrations of magnetite pristine shows a decrease in the cell viability of HaCat lineage. In contrast, Fe_3O_4 nanoparticles exhibited lower cell viability and the largest cytotoxicity to melanoma cells when compared to healthy cells. For these *in vitro* assays, all dilutions of magnetite caused the decrease of viability with statistical significance ($p < 0.05$*, and $p < 0.001$***, respectively), as can observed in the graph (Fig. 8b).

3.2.3 Lactate dehydrogenase assay

The effect of magnetic nanoparticles on cell membrane integrity was measured using the lactate dehydrogenase assay, as shown in Fig. 9 (a-b).

The LDH assay allows the assessment of cell damage caused by the release of the enzyme lactate dehydrogenase from lysed cells by rupture of the cell membrane. For the HaCat lineage, the LDH assay confirmed low cytotoxicity for all treatments and dilutions with the maintenance of membrane integrity

similarly the negative control, with a significant difference only at the highest concentration of EUG·Fe_3O_4 1:10 ($p < 0.01$**) [23].

The lactate dehydrogenase results on the A375 cell line demonstrated that only the highest concentrations of all treatments caused slightly enzyme release for the extracellular medium (considered statically significant, $p < 0.05$* and $p < 0.01$**) [24].

The release of LDH by cell lines (HaCat and A375) after 24 h of contact with different dilutions of magnetite pristine is shown in Fig. 10 (a-b).

The results of the LDH assay show that treatment of magnetite does not induce the release of enzyme LDH from the intracellular to the extracellular medium maintaining the cell integrity of the two cell lines tested.

A significant decrease in survival after the incubation time with the different treatments was found only at the highest concentrations tested, and even more expressive results can be observed in the tumor cell line.

Similar results of Fe_3O_4 pristine cytotoxicity in human epidermal keratinocytes were reported by Amin et al. [25]. According to experimental data, iron oxide nanoparticles are safe and biocompatible in high concentrations. Meantime, the cytotoxicity on the human melanoma cell line did not show a linear dependence with the proportion of Fe_3O_4 incorporated in eugenol and dilutions of treatments (EUG·Fe_3O_4 1:1, EUG·Fe_3O_4 1:5, and EUG·Fe_3O_4 1:10). However, A375 cells demonstrate sensitivity to treatments, even at the lowest concentration tested.

Farcas et al [26] developed a study to assess the cytocompatibility/cytotoxicity of Fe_3O_4 microparticles. The results reveal that the toxic effects on healthy cell lines and melanoma occur in a dose-dependent manner, and the mechanism involved in the decrease in cell viability is the induction of the apoptotic pathway.

It is shown in the literature that eugenol exhibits antitumor effects against several cell lines through different mechanisms. Regarding the cytotoxicity of eugenol, as it can be observed a decrease in the cell viability of a dose-dependent manner.

Al Wafai et al. [27] reported that MCF-7 cell lines are chemosensitive at low concentrations of eugenol. Furthermore, it was observed that cytotoxicity occurred not only due to mitochondrial dysfunction but also due to loss of plasma membrane integrity. Additionally, the apoptotic molecular mechanism of EUG for melanoma also has been supported and mentioned by several studies [28, 29].

3.2.4 IC_{50} values of HaCat and A375 cell lines

The IC_{50} is the concentration of nanoparticles required for resulting in a 50% decrease in cell numbers compared to untreated controls. The results of IC_{50} for the different treatments and cell lines are shown in

Table 1.

Table 1
IC_{50} evaluation of different compounds in HaCat and A375 lineages

Treatments	HaCat	A375
Fe_3O_4	226.08 μg.mL^{-1}	147.51 μg.mL^{-1}
EUG	79.08 μg.mL^{-1}	55.65 μg.mL^{-1}
EUG·Fe_3O_4 1:1	184.11 μg.mL^{-1}	242.22 μg.mL^{-1}
EUG·Fe_3O_4 1:5	346.84 μg.mL^{-1}	125.22 μg.mL^{-1}
EUG·Fe_3O_4 1:10	183.03 μg.mL^{-1}	112.87 μg.mL^{-1}

According to the IC_{50} values (Table 1), the free EUG was considered more toxic against the A375 cell line (55.65 μg.mL^{-1}) than for the keratinocyte cell lines (79.08 μg.mL^{-1}). Furthermore, it is also observed that tumor cells were more susceptible to treatments with magnetic nanoparticles when compared to normal cells, except for EUG·Fe_3O_4 1:1, which showed higher cytotoxicity for the HaCat cell line (IC_{50} =184.11 μg.mL^{-1}).

In addition, it is possible to verify that the magnetite-functionalization with eugenol raised the IC_{50} value of free eugenol, suggesting that the synergistic effect of the compounds decreases the cytotoxicity of the free oil to healthy cells.

Recently, Shahabadi et al. [7] developed magnetic nanoparticles coated silica and functionalized with eugenol for biological activity. The compound showed IC_{50} of 150.21 μg.mL^{-1} for U-87MG (human glioblastoma astrocytoma), 50.26 μg.mL^{-1} for A-549 (human lung carcinoma), and 25.34 μg.mL^{-1} for A-2780 (human ovarian carcinoma).

Diverse studies have been proposing some mechanisms of cytotoxicity of the eugenol in tumor cells, for instance, Jaganthan et al. [30] and Ghost et al. [31] report that effect against colon cancer and melanoma occurs by antiproliferative effect and induction of apoptosis. Regarding iron oxide nanoparticles, the mechanisms described are the generation of reactive oxygen species, inhibition of chemoresistant proteins, impairment of mitochondrial function, damage of DNA, and increase of apoptotic signals [32, 33].

The safety profile study performed using the HaCat lineage demonstrates that the nanoparticles proved to be biocompatible due to cell viability remaining around 80% according to ISO 10993-12 2009 [34].

3.3 Antibacterial and Antibiofilm activity

3.3.1 Disc diffusion

After the incubation, the inhibition zones were measured with digital caliper. The results of free eugenol, magnetite pristine, EUG·Fe_3O_4 1:1, EUG·Fe_3O_4 1:5 and EUG·Fe_3O_4 1:10 are shown in Table 2.

Table 2
Inhibition zone diameters formed after treatment (mm).

Bacterial strain	EUG	Fe_3O_4	EUG·Fe_3O_4 1:1	EUG·Fe_3O_4 1:5	EUG·Fe_3O_4 1:10
S. aureus	10.0 ± 1 mm	-	7.0 ± 1 mm	-	-
P. aeruginosa	7.0 ± 1 mm	-	7.0 ± 1 mm	-	-
E. coli	8.0 ± 1 mm	-	6.0 ± 1 mm	-	-
E. faecalis	6.0 ± 1 mm	-	-	-	-

According to the results, it is possible to verify that free eugenol has a broad spectrum against pathogenic microorganisms. In this regard, the bacterial strain *S. aureus* demonstrated the most susceptible, and *E. faecalis* is the most resistant. On the other hand, among the magnetic compounds, only EUG·Fe_3O_4 1:1 showed antimicrobial activity. The presence of an inhibition zone indicates a biocidal effect of the compounds that may implicate disruption of the bacterial cell membrane [35]

The sensibility to treatments depends on some factors, as the concentration of the substance, size particle, solubility, and bacterial concentration. As demonstrated on the topic of hydrodynamic size of the magnetite-functionalized eugenol (Fig. 4), the amount of the iron precursor employed in the reaction increased the size of magnetic nanoparticles [3], which is possibly related to the results obtained in the study of antibacterial activity. A larger surface area and smaller diameter particle enable better interaction with bacterial cells, increasing permeability and adhesion in the cell membrane, facilitating rupture and release of intracellular content [36].

Previous studies reported different mechanisms to the antibacterial activity of eugenol, which includes alteration of fatty acids, changes in morphology, and the cytoplasmatic membrane. Further, it can also cause ions transport modification, production of reactive oxygen species [37], and binding of the hydroxyl group with proteins, inhibiting bacterial enzymatic action [38, 39].

While the action mechanisms of MNPs can be attributed to the production of free radicals, such as hydrogen peroxide (H_2O_2) and superoxide anion ($O_2^{\cdot}$), causing intense oxidative stress, resulting in the degradation of vital substances for bacterial survival, such as lipids, proteins, and nucleic acids [40, 41].

3.3.2 Minimal inhibitory and bactericidal concentration

With the addition of the reagent, it was possible to verify visible microbial growth and determine the MIC. The MBC was observed after the incubation of seeded Nutrient agar plates. The MBC and MIC were demonstrated in Table 3.

Table 3
Minimal inhibitory and bactericidal concentration (mg.mL^{-1})

Bacterial strain	EUG		Fe_3O_4		EUG·Fe_3O_4 1:1		EUG·Fe_3O_4 1:5		EUG·Fe_3O_4 1:10	
	MIC	MBC	MIC	MBC	MIC	MBC	MIC	MBC	MIC	MBC
S. aureus	1.25	5.0	-	-	2.5	5.0	5.0	-	5.0	-
P. aeruginosa	1.25	2.5	-	-	0.62	0.62	5.0	-	5.0	-
E. coli	0.62	2.5	-	-	5.0	5.0	5.0	-	5.0	-
E. faecalis	2.5	-	-	-	5.0	-	5.0	-	5.0	-

The MIC values of free EUG for bacterial strains ranged from 0.62 mg.mL^{-1} to 2.5 mg.mL^{-1}, with the MBC measured to be approximately double the MIC. For the treatment with Fe_3O_4 pristine, no inhibitory/bactericidal activity against Gram-positive and Gram-negative bacteria used in this study it was observed.

The antimicrobial assay demonstrated that MIC values of EUG·Fe_3O_4 1:1 nanoparticle are different among tested bacterial strains. For *E. coli* and *E. faecalis*, the MIC value was the highest among the four tested species (5.0 mg.mL^{-1}). The MIC value for *S. aureus* was 2.5 mg.mL^{-1}, while for the *P. aeruginosa*, the lowest concentration able to inhibit the bacterial growth was 0.62 mg.mL^{-1}. Similar results were reported by Negut et al. [42] when using *Nigella sativa* functionalized Fe_3O_4 nanoparticles in different microbial strains.

No difference was observed in MIC values between EUG·Fe_3O_4 1:5 and EUG·Fe_3O_4 1:10 for all strains tested. However, these nanoparticles did not show the MBC values. The higher MIC values for magnetic nanoparticles with the highest amount of magnetite (EUG·Fe_3O_4 1:5 and EUG·Fe_3O_4 1:10) may be related to the lower amount of eugenol present in the sample (mass: mass ratio), which can be justified by the absence of biological activity of the nanoparticle pristine (Fe_3O_4). Likewise, Mohamed et al. [43] reported that plain Fe_3O_4 showed low antibacterial activity against *P. aeruginosa* (PAO1) and clinical isolates, considering the high MIC values.

3.3.3 Quantification of biofilm biomass

After the treatment, the biomass biofilm was quantified by crystal violet assay. The results inhibit the growth of biofilm using free eugenol and EUG·Fe_3O_4 1:1 is showed in Fig. 11.

The experiments demonstrate that free eugenol exhibits a low antibiofilm effect, while for EUG·Fe_3O_4 1:1 causes a significant decrease in biofilm biomass when compared to the positive control. A synergistic effect of magnetite and eugenol nanoparticles can be observed for *P. aeruginosa*, corroborating the results presented in Table 3.

The antibacterial and antibiofilm activity of eugenol is widely known in the literature. The antibacterial effects are associate to increase cell permeability, disruption of the cytoplasmic membrane, and modification of shape cell [43, 44]. Meanwhile, antibiofilm activity occurs through cell lysis, disruption of the cell-cell junction, and inhibition of the quorum detection system [45, 46].

4 Conclusions

In this work, we reported the preparation of EUG·Fe_3O_4 with different proportions of Fe_3O_4 incorporated via the co-precipitation method employing only one iron precursor ($FeSO_4$). Through a simple methodology and under very mild conditions, the eugenol incorporated magnetite was fully characterized by infrared spectroscopy, X-ray diffractogram, and scanning electron microscopy, as well as by approximation of an external magnetic field. It was also found that the magnetite-functionalization eugenol caused changes in crystallinity of Fe_3O_4 and average particle size. The evaluation of the safety and cytotoxic profile performed by the MTT, NR, and LDH assay showed that the magnetic compounds demonstrate cytocompatibility and exhibit higher toxicity in tumor cells comparing the non-magnetic analogue. Moreover, increasing the proportion and concentration of iron increases cell toxicity, as verified from the IC_{50} values. The antibacterial assay evidenced the antibacterial activity of free eugenol and EUG·Fe_3O_4 1:1 against *S. aureus*, *E. coli*, *E. faecalis*, and *P. aeruginosa* were similar. In the meantime, the EUG·Fe_3O_4 1:1 demonstrate more effectiveness in inhibiting the bacterial biofilm when compared to free eugenol. Nevertheless, the controlled incorporation of magnetite on the eugenol surface shows to be an effective tool for futures studies for biological applications in essential oil drug derivatives.

Declarations

Acknowledgements. The authors would like to thank Coordenação de Aperfeiçoamento de Pessoal de Nível Superior – Brasil (CAPES) – Finance Code 001, FAPERGS, CNPq, Laboratório de Materiais Magnéticos Nanoestruturados (LaMMaN), and Universidade Franciscana for the support.

Conflict of interest. The authors declare no competing interests

References

1. M. Chidambaram, R. Manavalan, K. Kathiresan, Nanotherapeutics to overcome conventional cancer chemotherapy limitations. J. Pharm. Pharm. Sci. **14**, 67–77 (2011)
2. S.Y. Wang, H.Z. Hu, X.C. Qing, Z.C. Zhang, Z.W. Shao, Recent advances of drug delivery nanocarriers in osteosarcoma treatment. J. Cancer. **1**, 69–82 (2020)
3. C.R.B. Rhoden, F.S. Bruckmann, T.R. Salles, C.G. Kaufmann Jr., S.R. Mortari, Study from the influence of magnetite onto removal of hydrochlorothiazide from aqueous solutions applying magnetic graphene oxide. J. Water. Process. Eng. **43**, 102262 (2021). https://doi.org/10.1016/j.jwpe.2021.102262

4. A.R. Viana, B. Salles, F.S. Bruckmann, L.M.F. Krause, S.R. Mortari, C.R.B. Rhoden, Cytotoxicity study of graphene oxide against vero lineage cells. Discip. Sci. Sér. Ciên. Nat. Tecnol. **20**, 355–364 (2019)
5. T.R. Salles, H.B. Rodrigues, F.B. Bruckmann, L.C.S. Alves, S.R. Mortari, C.R.B. Rhoden, Graphene oxide optimization synthesis for application on laboratory of Universidade Franciscana. Discip. Sci. Sér. Ciên. Nat. Tecnol. **21**, 15–26 (2020)
6. M. Mohajeri, B. Behnam, A. Sahebkar, Biomedical applications of carbon nanomaterials: drug and gene delivery potentials. J. Cell. Phys. **234**, 298–319 (2019)
7. N. Shahabadi, A. Akbari, F. Karampour, M. Falsafı, Cytotoxicity and antibacterial activities of new chemically synthesized magnetic nanoparticles containing eugenol. J. Drug. Del. Sci. Technol. **49**, 113–122 (2019)
8. F.S. Bruckmann, A.C. Pimentel, A.R. Viana, T.R. Salles, L.M.F. Krause, S.R. Mortari, C.R.B. Rhoden, Synthesis, characterization and cytotoxicity evaluation of magnetic nanosilica in L929 cell line. Discip. Sci. Sér. Ciên. Nat. Tecnol. **21**, 1–14 (2020)
9. R. Vakili-Ghartavol, A.A. Momtazi-Borojeni, Z. Vakili-Ghartavol, H.T. Aiyelabegan, M.R. Jaafari, S.M. Rezayat, S. Arbabibidgoli, Toxicity assessment of superparamagnetic iron oxide nanoparticles in different tissues. Artif. Cells. Nanomed. Biotechnol. **48**, 443–451 (2020)
10. L.H. Reddy, J.L. Arias, J. Nicolas, P. Couvreur, Magnetic nanoparticles: design and characterization, toxicity and biocompatibility, pharmaceutical and biomedical applications. Chem. rev. **112**, 5818–5878 (2012)
11. E. Talón, M. Vargas, A. Chiralt, C. González-Martínez, Antioxidant starch-based films with encapsulated eugenol. Application to sunflower oil preservation. Lwt. **113**, 108290 (2019)
12. F. Esmaeili, S. Rajabnejhad, A.R. Partoazar, S.E. Mehr, R. Faridi-Majidi, M. Sahebgharani, L. Syedmoradi, M.R. Rajabnejhad, A. Amani, Anti-inflammatory effects of eugenol nanoemulsion as a topical delivery system. Pharm. Dev. Technol. **21**, 887–893 (2016)
13. T. Mosmann, Rapid colorimetric assay for cellular growth and survival: Application to proliferation and cytotoxicity assays. J. Immunol. Methods. **65**, 55–63 (1983)
14. E. Borenfreund, J.A. Puerner, Toxicity determined in vitro by morphological alterations and neutral red absorption. Toxicol. Lett. **24**, 119–124 (1985)
15. A.W. Bauer, W.M. Kirby, J.C. Sherris, M. Turck, Antibiotic susceptibility testing by a standardized single disk method. Am. J. Clin. Pathol. **45**, 493–496 (1966)
16. CLSI, *Methods for Dilution Antimicrobial Susceptibility Tests for Bacteria That Grow Aerobically; Approved Standard-Tenth Edition. CLSI DOCUMENTE M07-A10* (Clinical and Laboratory Standards Institute, In Wayne, PA, 2015)
17. S. Manner, M. Skogman, D. Goeres, P. Vuorela, A. Fallarero, Systematic exploration of natural and synthetic flavonoids for the inhibition of Staphylococcus aureus biofilms. Int. J. Mol. Sci. **14**, 19434–19451 (2013)
18. L.Q.S. Lopes, C.G. Santos, R.A. Vaucher, R.P. Raffin, R.C.V. Santos, Nanocapsules with glycerol monolaurate: Effects on Candida albicans biofilms. Microb. Pathog. **97**, 119–124 (2016)

19. K. Pramod, C.V. Suneesh, S. Shanavas, S.H. Ansari, J. Ali, Unveiling the compatibility of eugenol with formulation excipients by systematic drug-excipient compatibility studies. J. Anal. Sci. Technol. **6**, 1–14 (2015)
20. K.J. Datta, A.K. Rathi, V. Kumar, J. Kaslik, I. Medrik, V. Ranc, R.S. Varma, R. Zboril, M.B. Gawande, Synthesis of flower-like magnetite nanoassembly: application in the efficient reduction of nitroarenes. Sci. Rep. **7**, 1–12 (2017)
21. S. Tanaka, Y.V. Kaneti, N.L.W. Septiani, S.X. Dou, Y. Bando, M.S.A. Hossain, J. Kim, Y. Yamauchi, A Review on Iron Oxide-Based Nanoarchitectures for Biomedical, Energy Storage, and Environmental Applications. Small Methods. **3**, 1800512 (2019). https://doi.org/10.1002/smtd.201800512
22. P.A. Hartley, G.D. Parfitt, L.B. Pollack, The role of the van der Waals force in the agglomeration of powders containing submicron particles. Powder Technol. **42**, 35–46 (1985)
23. M. Gonzales, L.M. Mitsumori, J.V. Kushleika, M.E. Rosenfeld, K.M. Krishnan, Cytotoxicity of iron oxide nanoparticles made from the thermal decomposition of organometallics and aqueous phase transfer with Pluronic F127. Contrast. Media. Mol. imaging. **5**, 286–293 (2010)
24. E. Catalano, In vitro biological validation and cytocompatibility evaluation of hydrogel iron-oxide nanoparticles. AIP Conference Proceedings. **1873**, 020011 (2017) https://doi.org/10.1063/1.4997140
25. R. M. Amin, A. Abdelmonem, T. Verwanger, E. Elsherbini, B. Krammer, Cytotoxicity of magnetic nanoparticles on normal and malignant human skin cells. Nano Life. **4**, 1440002 (2014) https://doi.org/10.1142/S1793984414400029
26. C. G. Farcas, I. Macasoi, I. Pinzaru, M. Chirita, M. C. Chirita Mihaila, C. Dehelean, S. Avram, F. Loghin, L. Mocanu, V. Rotaru, A. Ieta, A. Ercuta, D. Coricovac, Controlled synthesis and characterization of micrometric single crystalline magnetite with superparamagnetic behavior and cytocompatibility/cytotoxicity assessments. Front. Pharmacol. **11**, 410 (2020) https://doi.org/10.3389/fphar.2020.00410
27. R. Al Wafai, W. El-Rabih, M. Katerji, R. Safi, M. El Sabban, O. El-Rifai, J. Usta, Chemosensitivity of MCF-7 cells to eugenol: release of cytochrome-c and lactate dehydrogenase. Sci. Rep. **7**, 1-13 (2017)
28. M. Pisano, G. Pagnan, M. Loi, M. E. Mura, M. G. Tilocca, G. Palmieri, D. Fabbri, M. A. Dettori, G. Delogu, M. Ponzoni, C. Rozzo, Antiproliferative and pro-apoptotic activity of eugenol-related biphenyls on malignant melanoma cells. Mol. cancer. **6**, 1-12 (2007)
29. S. K. Jaganathan, E. Supriyanto, Antiproliferative and molecular mechanism of eugenol-induced apoptosis in cancer cells. Molecules. **17**, 6290-6304 (2012)
30. S.K. Jaganathan, A. Mazumdar, D. Mondhe, M. Mandal, Apoptotic effect of eugenol in human colon cancer cell lines. Cell. Biol. Int. **35**, 607–615 (2011)
31. R. Ghosh, N. Nadiminty, J.E. Fitzpatrick, W.L. Alworth, T.J. Slaga, A.P. Kumar, Eugenol causes melanoma growth suppression through inhibition of E2F1 transcriptional activity. J. Biol. Chem. **280**, 5812–5819 (2005)

32. J.A. Jacob, J.M.M. Salmani, B. Chen, Magnetic nanoparticles: mechanistic studies on the cancer cell interaction. Nanotechnol. Rev. **5**, 481–488 (2016)
33. R.A. Revia, M. Zhang, Magnetite nanoparticles for cancer diagnosis, treatment, and treatment monitoring: recent advances. Mater. Today. **19**, 157–168 (2016)
34. ISO, *10993-12. Biological evaluation of medical devices. Part 12: sample preparation and reference materials* (International Organization for Standardization, ed. Geneva, Switzerland, 2009)
35. P.S.X. Yap, K. Yusoff, S.H.E. Lim, C.M. Chong, K.S. Lai, Membrane Disruption Properties of Essential Oils—A Double-Edged Sword?. Processes. **9**, 595 (2021). https://doi.org/10.3390/pr9040595
36. L. Zhang, P.Y. Tan, C.L. Chow, C.K. Lim, O.K. Tan, M.S. Tse, C.C. Sze, Antibacterial activities of mechanochemically synthesized perovskite strontium titanate ferrite metal oxide. Colloids. Surf. A: Physicochem. Eng. Asp. **456**, 169–175 (2014)
37. B. Das, D. Mandal, S.K. Dash, S. Chattopadhyay, S. Tripathy, D.P. Dolai, S.K. Dey, S. Roy, Eugenol provokes ROS-mediated membrane damage-associated antibacterial activity against clinically isolated multidrug-resistant Staphylococcus aureus strains. Infect. Dis. Res. Treat. **9**, S31741 (2016). https://doi.org/10.4137/IDRT.S31741
38. F. Nazzaro, F. Fratianni, L. De Martino, R. Coppola, V. De Feo, Effect of essential oils on pathogenic bacteria. Pharmaceuticals. **6**, 1451–1474 (2013)
39. R.A. Ismail, G.M. Sulaiman, S.A. Abdulrahman, T.R. Marzoog, Antibacterial activity of magnetic iron oxide nanoparticles synthesized by laser ablation in liquid. Mater. Sci. Eng. C. **53**, 286–297 (2015)
40. S. Ma, S. Zhan, Y. Jia, Q. Zhou, Superior antibacterial activity of Fe3O4-TiO2 nanosheets under solar light. ACS Appl. Mat. Interfaces. **7**, 21875–21883 (2015)
41. A. Marchese, R. Barbieri, E. Coppo, I.E. Orhan, M. Daglia, S.F. Nabavi, M. Izadi, M. Abdollahi, M.S. Nabavi, M. Ajami, Antimicrobial activity of eugenol and essential oils containing eugenol: A mechanistic viewpoint. Crit. Rev. Microbiol. **43**, 668–689 (2017)
42. I. Negut, V. Grumezescu, A. Ficai, A.M. Grumezescu, A.M. Holban, R.C. Popescu, D. Savu, G. Socol, MAPLE deposition of Nigella sativa functionalized Fe3O4 nanoparticles for antimicrobial coatings. Appl. Surf. Sci. **455**, 513–521 (2018)
43. H.B. Mohammed, S.M.I. Rayyif, C. Curutiu, A.C. Birca, O.C. Oprea, A.M. Grumezescu, L.M. Ditu, I. Gheorghe, M.C. Chifiriuc, G. Mihaescu, A. M. Holban, Eugenol-Functionalized Magnetite Nanoparticles Modulate Virulence and Persistence in Pseudomonas aeruginosa Clinical Strains. Molecules. **26**, 2189 (2021). https://doi.org/10.3390/molecules26082189
44. M.K. Yadav, S.W. Chae, G.J. Im, J.W. Chung, J.J. Song, Eugenol: a phyto-compound effective against methicillin-resistant and methicillin-sensitive Staphylococcus aureus clinical strain biofilms. PLoS One. **10**, e0119564 (2015). https://doi.org/10.1371/journal.pone.0119564
45. N.A. Al-Shabib, F.M. Husain, I. Ahmad, M.H. Baig, Eugenol inhibits quorum sensing and biofilm of toxigenic MRSA strains isolated from food handlers employed in Saudi Arabia. Biotechnol. Biotechnol. Equip. **31**, 387–396 (2017)

46. Z. Lou, K.S. Letsididi, F. Yu, Z. Pei, H. Wang, V. Letsididi, Inhibitive effect of eugenol and its nanoemulsion on quorum sensing–mediated virulence factors and biofilm formation by Pseudomonas aeruginosa. J. Food Prot. **82**, 379–389 (2019)

Figures

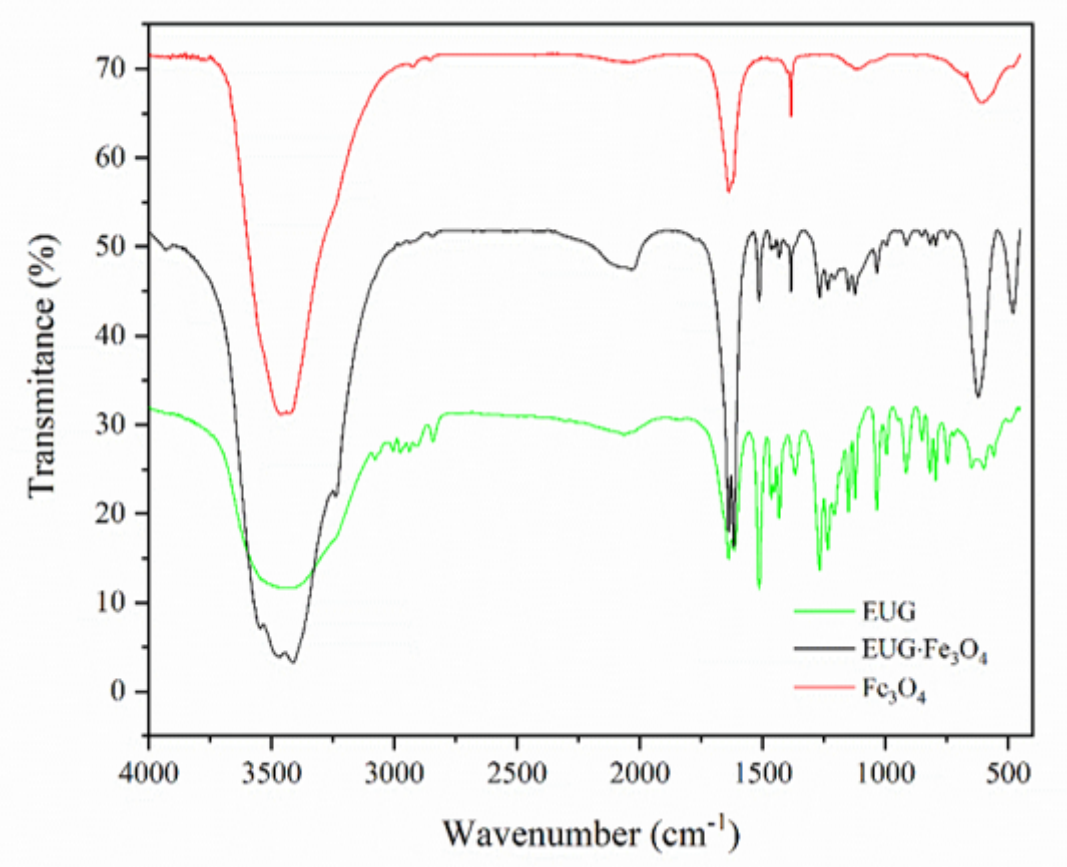

Figure 1

Infrared spectrum of magnetite, magnetite-functionalized eugenol, and eugenol, respectively

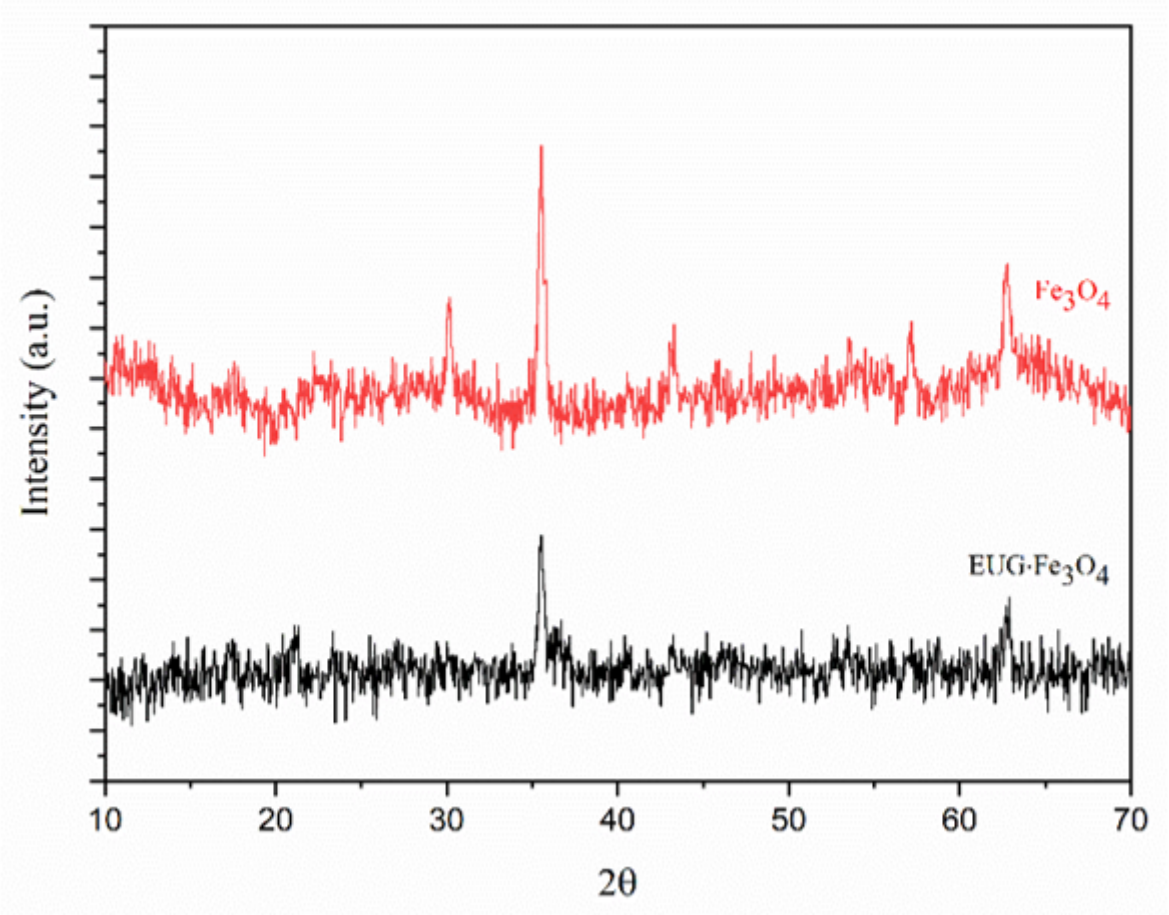

Figure 2

X-ray diffraction of magnetite and magnetite-functionalized eugenol

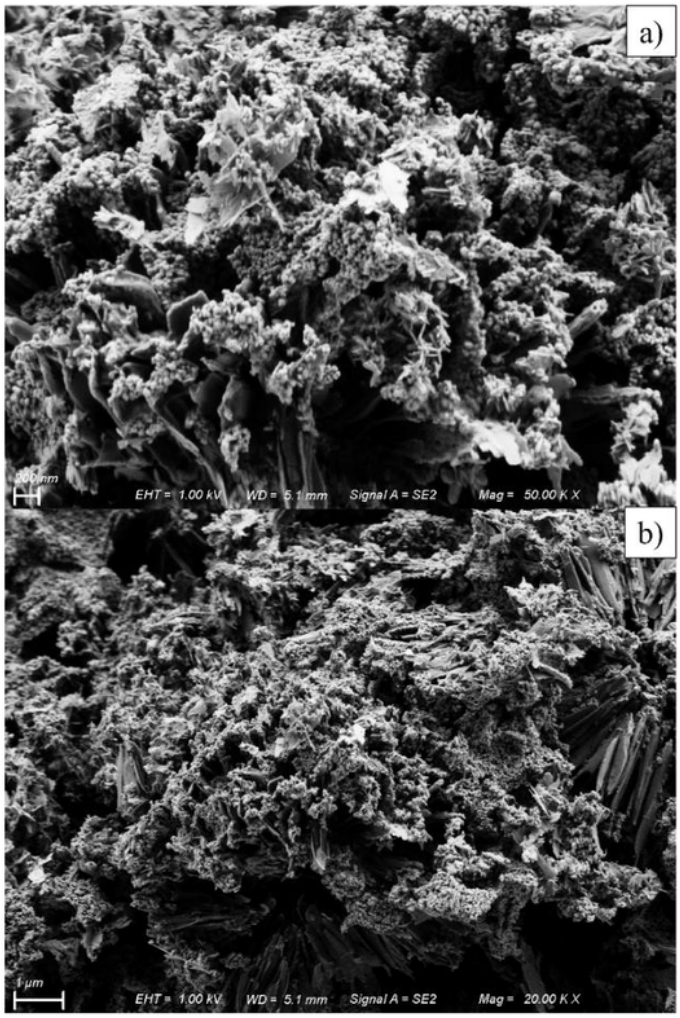

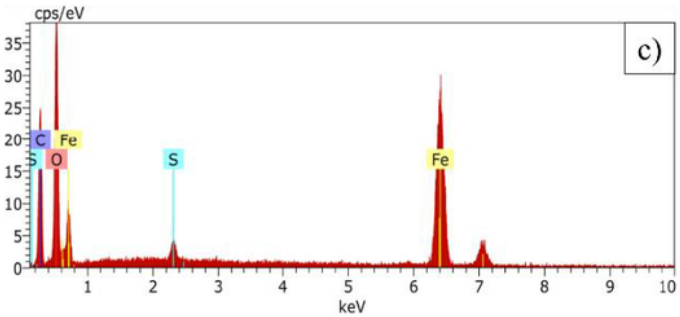

El	AN	Series	unn. C [wt.%]	norm. C [wt.%]	Atom. C [at.%]	Error (1 Sigma) [wt.%]
O	8	K-series	41.74	35.42	41.31	6.14
Fe	26	K-series	39.33	33.37	11.15	1.13
C	6	K-series	35.63	30.24	46.97	5.79
S	16	K-series	1.15	0.98	0.57	0.09
		Total:	117.85	100.00	100.00	

Figure 3

(a-b) SEM images, and (c) EDS of EUG·Fe3O4

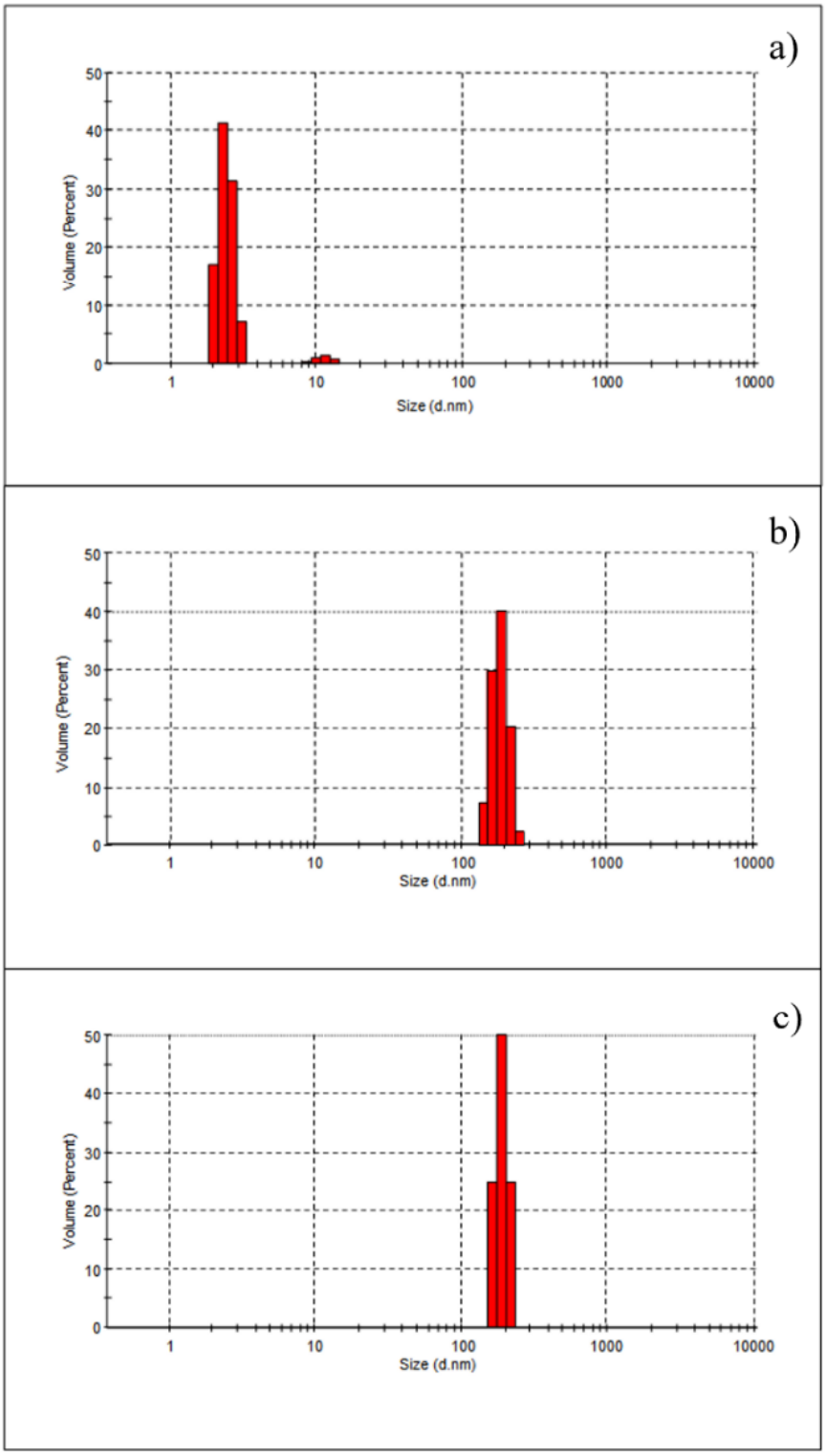

Figure 4

(a) Size distribution profiles of EUG·Fe3O4 1:1, (b) EUG·Fe3O4 1:5 and, (c) EUG·Fe3O4 1:10

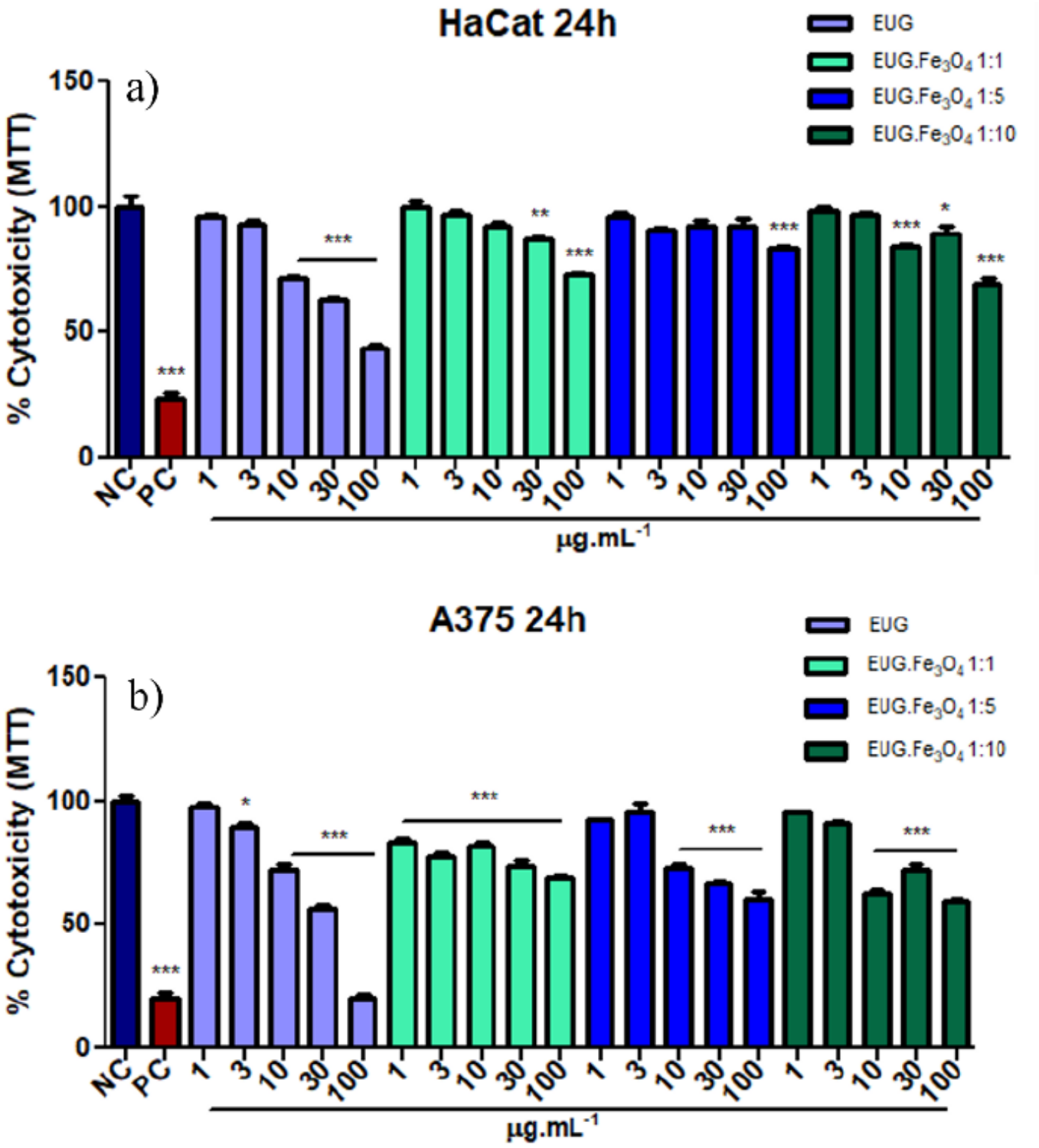

Figure 5

Cellular cytotoxicity of free EUG and magnetite-functionalized eugenol

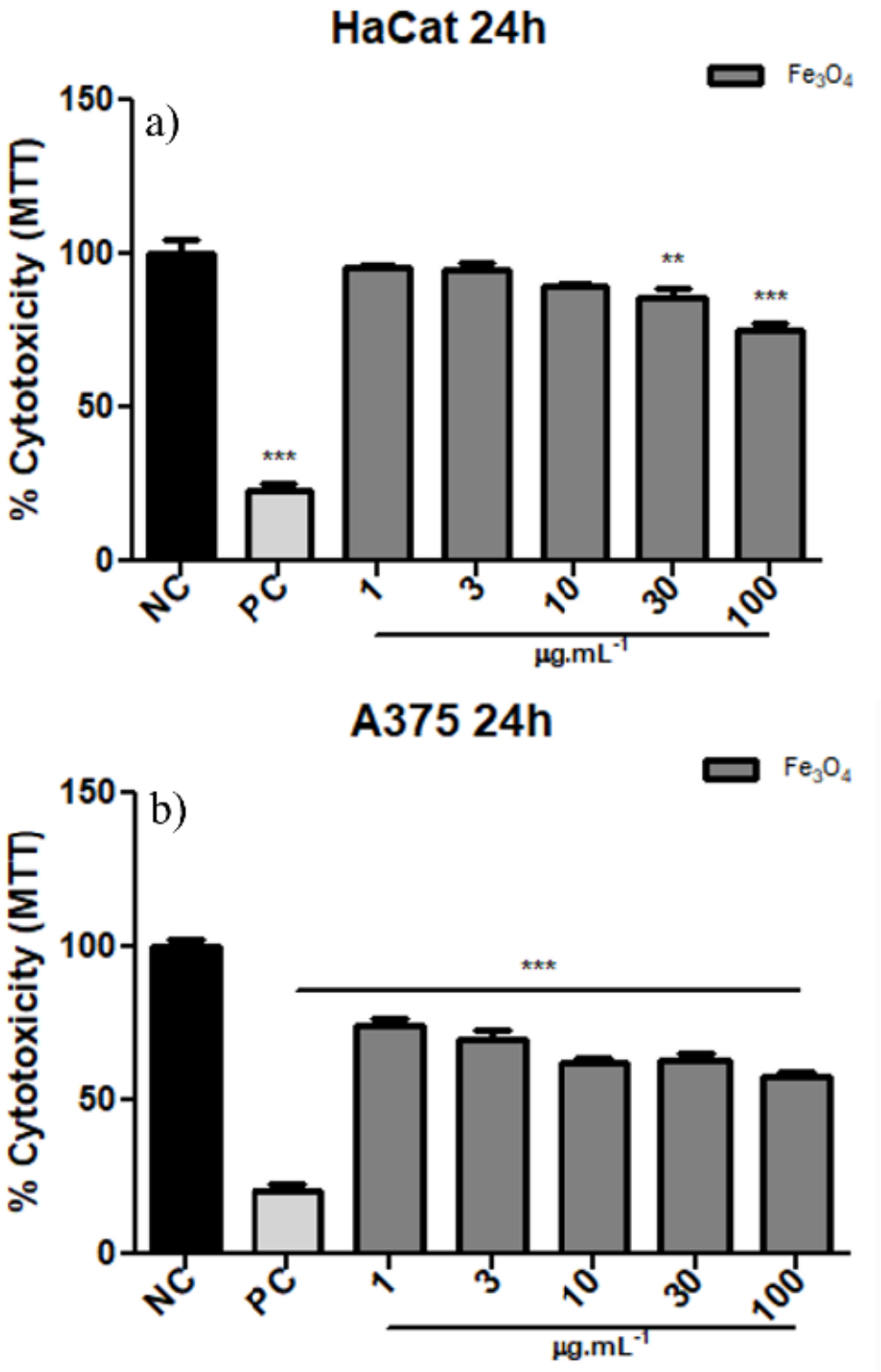

Figure 6

(a) Cell lines viability of HaCat, and (b) A375 with different concentrations of Fe3O4

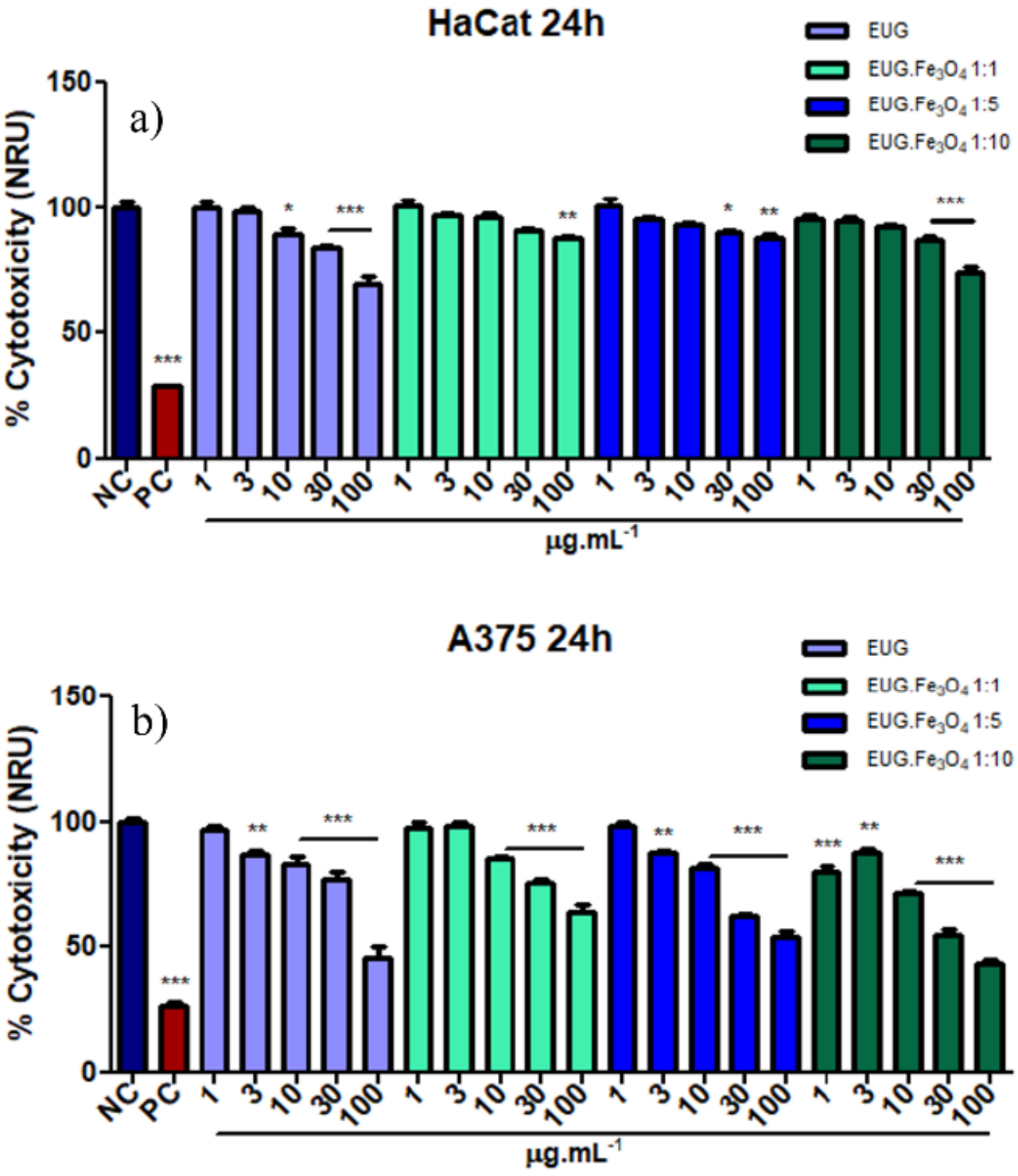

Figure 7

(a) Inhibition of keratinocyte, and (b) melanoma cell lines by free EUG and EUG·Fe3O4 after 24 h.

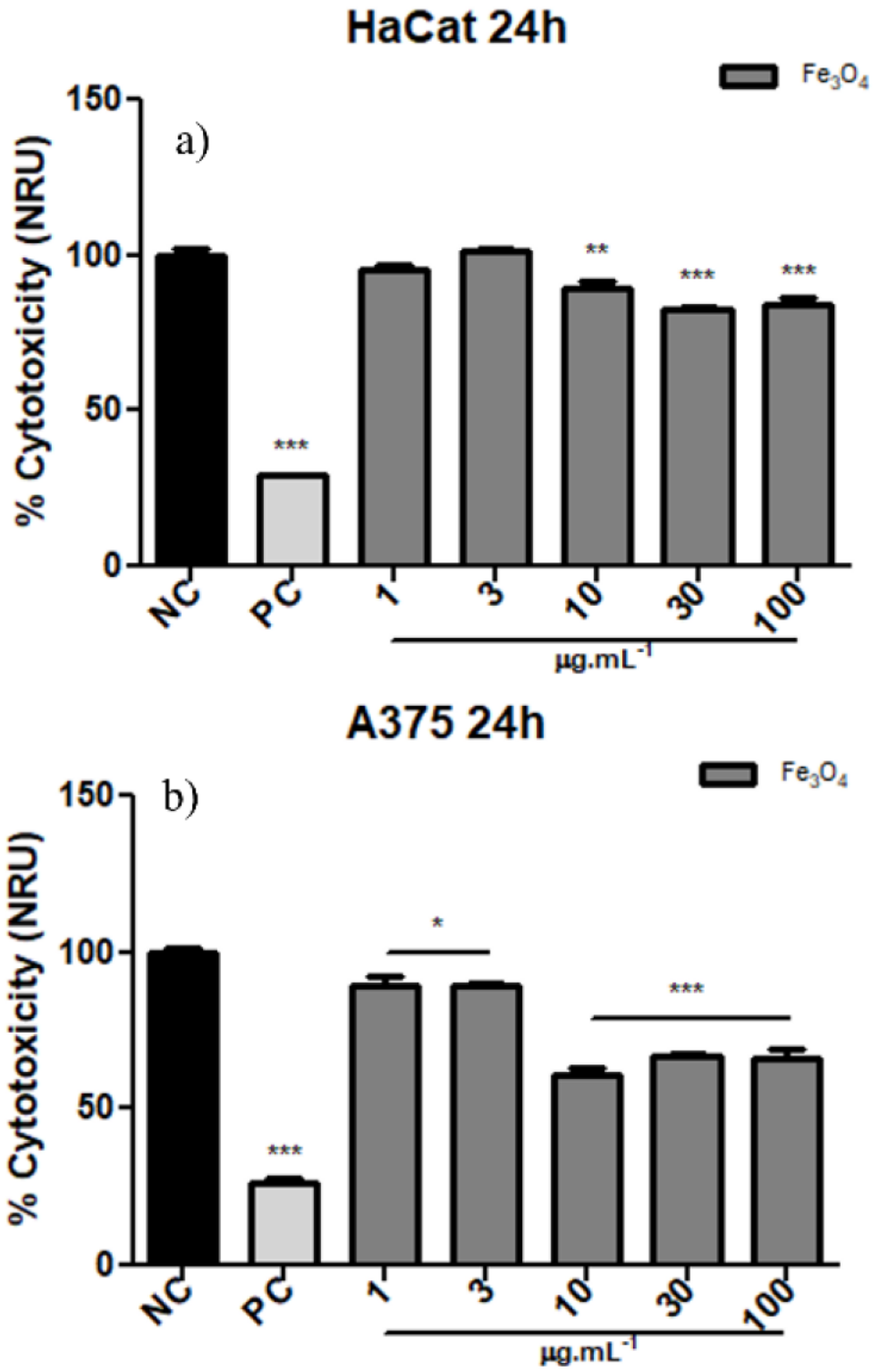

Figure 8

(a) Cell lines viability of HaCat, and (b) A375 with different concentrations of Fe3O4

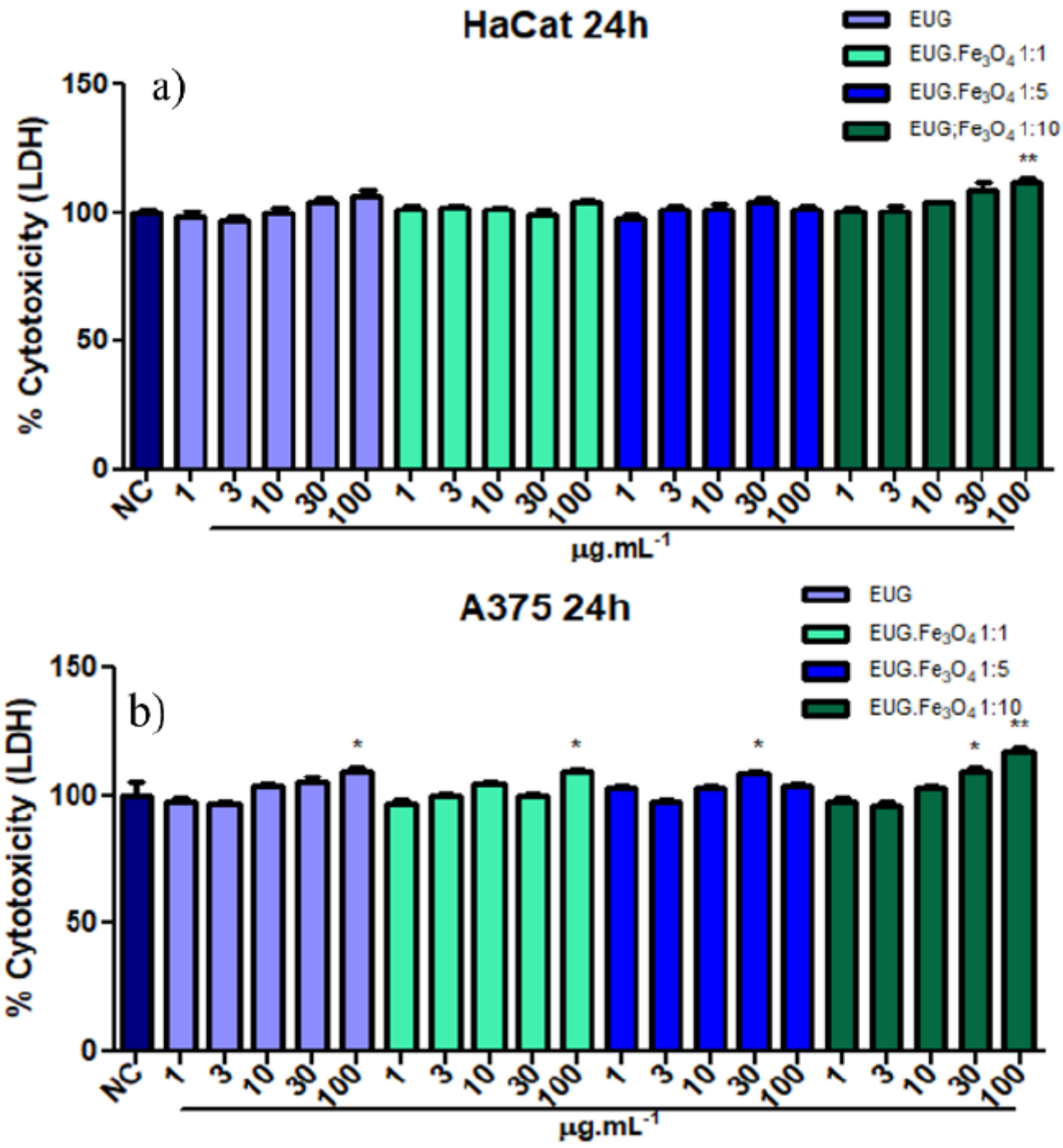

Figure 9

(a) Cytotoxicity of free eugenol and magnetite-functionalized eugenol against HaCat and (b) A375 cells assessed through lactate dehydrogenase assay

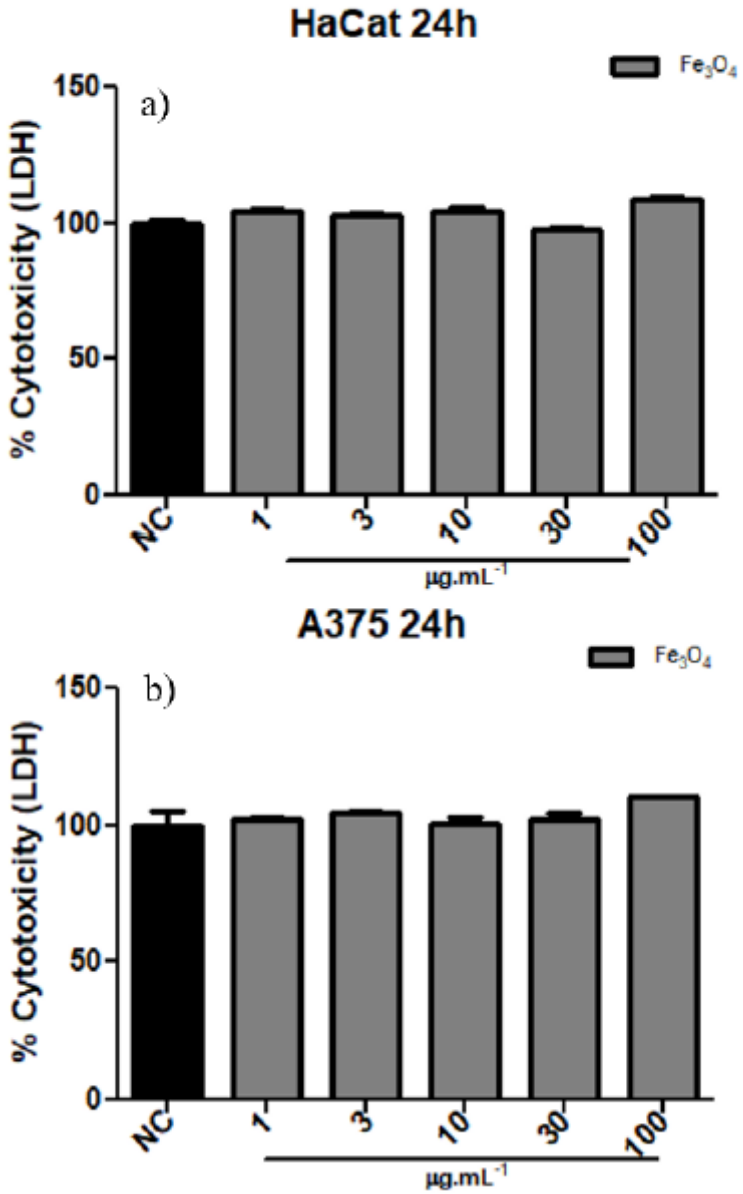

Figure 10

Effect of Fe3O4 on cell membrane integrity following exposure to different concentrations for 24 h

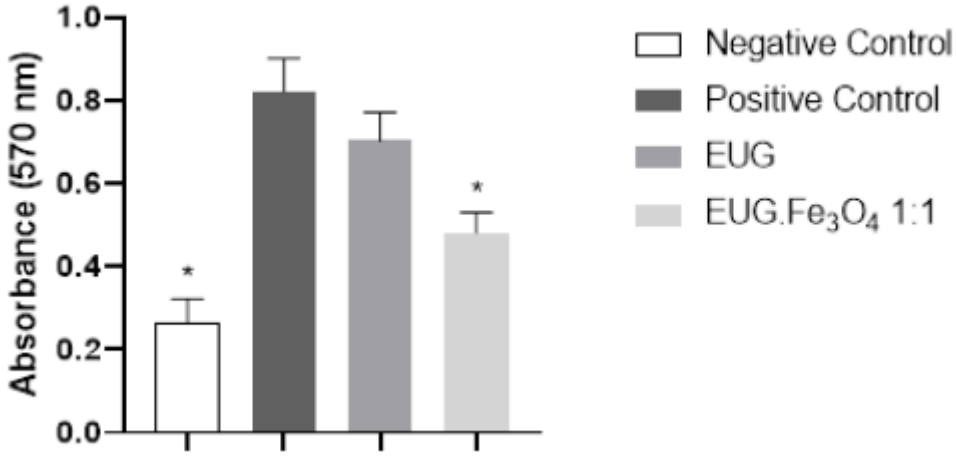

Figure 11

Quantification of biofilm biomass

Supplementary Files

This is a list of supplementary files associated with this preprint. Click to download.

- GraphicalAbstract.png